

Evaluating the Progression and Orientation of Scratches on Outer-Raceway Bearing Using Pattern Recognition Method

Shrinathan Esakimuthu Pandarakone, *Student Member*, Yukio Mizuno, *Member*, and Hisahide Nakamura, *Member*

Abstract— Bearing faults are a major source of failure in induction motor and early detection of fault becomes necessary because of its industrial application. A range of analytical methods has been used to detect, identify, and diagnose bearing faults, including vibrational analysis. Most analyses have used pitting as the fault, whereas in industrial environments, scratches are a more common problem. The present study investigated such scratches, applying two types of fault analysis: fault progression and fault orientation. A Support Vector Machine (SVM) algorithm was used to classify and diagnose the different types of bearing fault. The frequency domain features obtained from a fast Fourier transform (FFT) of the load current were used to train the SVM algorithm. The proposed diagnostic method was tested experimentally using induced outer race faults under different load conditions. The method was shown to be successful in diagnosing faults, suggesting potential applications in real industrial settings.

Index Terms— Bearings, fault diagnosis, induction motors, orientation, progression of scratches, spectral analysis, Support Vector Machine.

I. INTRODUCTION

ELECTRIC motor plays a role in almost every area of modern life, and induction motors are widely used in both domestic and industrial applications. They play a central role in a range of industries because of their lower power consumption. The use of induction motors has therefore been increasing. If faults arising in such motors are not identified at an early stage, output may be seriously affected. Appropriate monitoring is therefore needed to ensure that the motor has a long life and to maintain reliability and efficiency.

A defect in an electric motor is defined as a reduction in the capacity to perform a required function. If a defective motor is kept in operation for an extended period of time, it will exhibit

symptoms including increases in temperature, variation in the current harmonics, changes to the electromagnetic field, or vibration [1]. Failures in induction motors can be broadly divided into electrical and mechanical depending on their origin [2]. In the case of induction motors, bearings are the most common failure point (44%), followed by stators (26%) and rotors (8%) [3]. Faults arising in the bearings therefore play a key role in unplanned downtime [4]. They are the logical starting point in any attempt to increase reliability [5-7].

A range of techniques has been developed to predict bearing failure in induction motors [8-10]. In most cases, the fault arises from surface damage, and failure analysis is performed [11-13]. Vibration analysis is the most commonly used technique for identifying bearing faults [14-16]. This approach requires careful selection and placement of the sensors that record the vibration signal, and the introduction of digital signal processing has extended its range of applications [17]. Digital systems mainly rely on the use of artificial intelligence tools such as artificial neural networks [18], fuzzy logic, or expert systems [19]. Stator current analysis has also been extended to the detection of bearing failure [20-21]. Widely used techniques include squared envelope analysis [22], spectral kurtosis analysis [23], and the wavelet kurtogram [24], root mean square [25] analysis, high-order statistical methods [26], and the short impulse method [27]. In most cases, the raw signal cannot be used to identify a failure, and features must be extracted from time domain or frequency domain analysis. Time domain analysis allows processing of both stationary and non-stationary signals. Frequency domain analysis has high process gain and is less sensitive to noise in the signal. It can detect faults only from a stationary signal and cannot be applied to non-stationary signals [28].

In industrial applications, faults in induction motor bearings often arise from scratches. Few studies have investigated this phenomenon [29], and further research is required. The present study addresses scratching as a fault factor and analyzed two aspects of bearing failure: scratch progression and scratch orientation on the outer raceway of the bearing. The study is the first to investigate the frequency components of load current using fast Fourier transform (FFT) and to treat these as the main feature for analysis. A Support Vector Machine (SVM) algorithm, trained on the frequency domain features derived

Manuscript received November 08, 2017; revised February 15, 2018 and March 26, 2018; accepted April 19, 2018.

S. Esakimuthu Pandarakone and Y. Mizuno are with the Department of Electrical and Mechanical Engineering, Nagoya Institute of Technology, Nagoya, Aichi, 466-8555 Japan (e-mail: sarushrinathan@gmail.com, mizuno.yukio@nitech.ac.jp).

H. Nakamura is with the R&D Division, TOENEC Corporation, Nagoya, Aichi, 457-0819 Japan. (e-mail: hisahide-nakamura@toenec.co.jp).

from the FFT, was used to classify and diagnose the different types of bearing fault. The diagnosis did not require the rotating speed of the induction motor to be considered, making it appropriate for industrial environments. The progress of bearing faults and the orientation of scratches on the outer raceway of the bearing were studied in detail. The effectiveness of the proposed fault detection scheme in diagnosing faults at the outer race was investigated through experiments under different load conditions.

The rest of the paper is organized as follows. Section II describes the experimental setup. Section III briefly reviews the types of bearing fault considered in the study and discusses the effect of scratching. Sections IV and V introduce FFT analysis and feature extraction, respectively. Section VI presents the SVM diagnosis, and Section VII presents conclusions and proposed future work. Fig. 1 provides a flow analysis of the proposed method.

II. EXPERIMENTAL SETUP OF PROPOSED SYSTEM

The experimental setup is shown in Fig. 2 (a). The present study was carried out by considering powder brake as a mechanical load and it was coupled to the induction motor through coupling brushes. This powder brake allows the rotational speed of the induction motor to be varied. Speeds from 1780 to 1765 min^{-1} were used in the experiments. Under these conditions, the instantaneous load current of the stator was between 8 and 12 A . The load current was measured using current probes (HIOKI 9695-02), and the voltage of the stator winding was measured using voltage probes (HIOKI 9666). The rotational speed was monitored using a speed indicator (ONOSOKKI HT-5500). The output signal from the sensors were transferred to a desktop computer (PC) and recorded simultaneously using a system (Fig. 2 (b)) developed by the authors with the tolerance error of $\pm 2\%$. The full-scale measurement of current and voltages were 20 A and 300 V , respectively. The measurement system had seven input terminals and seven A/D converters. In the current study, the three-phase load currents, three line-to-line voltages, and rotational speed were recorded through the seven channels. Frequency analysis resolution is normally determined by the sampling time, and it is preferable to achieve high frequency resolution. The sampling time was therefore set at approximately $10 \mu\text{s}$, giving a frequency resolution of 0.76 Hz and a data recording length of 2^{17} per channel. Data were acquired at 30 s intervals, triggered by a timer. Data transfer across the seven channels took less than 20 s .

A three-phase induction motor (2.2 kW , 200 V , 8.5 A , 1740 min^{-1} , 4 poles) was used in the experiments. The stator winding has a double-star configuration. The power source had a frequency of 60 Hz . The power supply to the induction motor was fed directly from the main system. The bearing failures in the outer raceway were artificially introduced. The motor was tested under normal operation to provide reference data and then retested after bearing failure had been induced.

Only the U-phase load current of the stator was used in the failure analysis, but the phase voltage and load current of the V and W phases were recorded for reference. FFT analysis of the

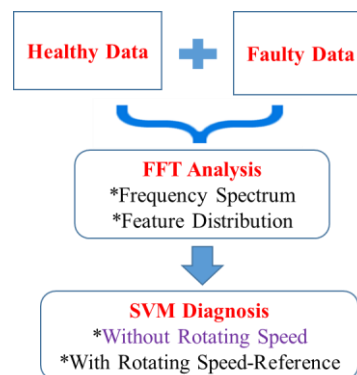
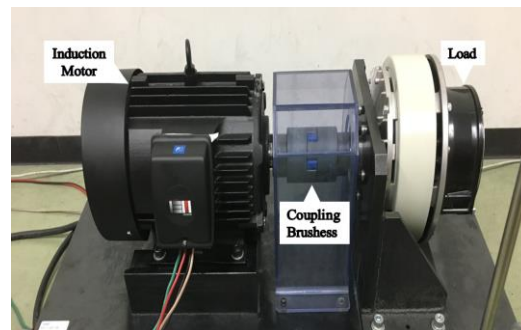


Fig. 1. Flowchart of bearing failure analysis.



(a) Experimental setup



(b) Measurement system

Fig. 2. Experimental setup and developed measurement system.

U-phase load current was performed under all bearing conditions. 283 fundamental wavelengths were used in FFT.

III. ARTIFICIAL SCRATCH DEFECTS CHARACTERIZATION

Two factors were analyzed: progression of a scratch on the bearing and the orientation of scratches on the outer raceway. If a scratch appearing on a bearing is not detected at an early stage, it may increase in size as the motor runs. To simulate this and to allow the progression of a fault on the outer raceway of the bearing to be analyzed, scratches with lengths of 5 , 10 , and 15 mm were induced. The depth and width of the scratches were held constant at 0.5 mm . Fault progression in one sample is shown in Fig. 3.

As the direction that a scratch will take on the bearing is inherently unpredictable, scratches 10 mm in length were induced in four orientations: horizontal, vertical, left, and right. These are shown in Fig. 4. In the case of the 5 mm horizontal scratch, no change was observed in the performance of the

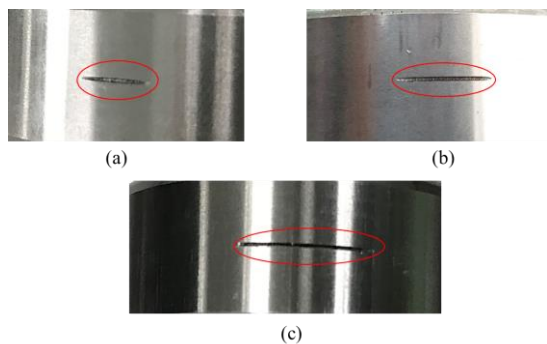


Fig. 3. Progressive bearing failure prototype (a) horizontal scratch 5 mm (b) horizontal scratch 10 mm (c) horizontal scratch 15 mm.

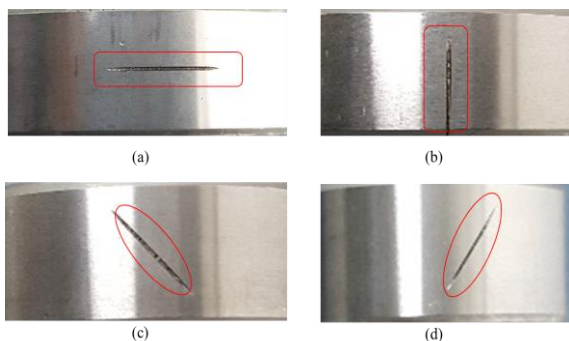


Fig. 4. Distinct orientation of 10 mm scratches (a) horizontal scratch (b) vertical scratch (c) right orientation scratch (d) left orientation scratch.

motor, and this was excluded from the orientation analysis. The 10 mm horizontal scratch produce large signal difference from the healthy condition and was selected for the orientation analysis.

The following terminology is used in the paper. H, HS, VS, LS, and RS denote the healthy condition, horizontal scratch, vertical scratch, left orientation scratch, and right orientation scratch conditions, respectively. The code is followed by the scratch length in mm. Thus, for example, a 10 mm horizontal scratch is denoted HS10.

IV. LOAD CURRENT FREQUENCY SPECTRUM ANALYSIS

The load current of the stator is the main component of bearing failure detection using the frequency spectrum. In this section, we discuss this approach to frequency spectrum analysis, its use in analyzing fault progression, and the role of orientation in bearing failure.

A. Spectral Analysis of Scratch Progression

FFT analysis of the U-phase load current was performed under all four bearing conditions. Figs. 5 and 6 compare the frequency spectra plotted for H–HS10 and HS5–HS10–HS15, respectively, at a rotating speed of 1765 min^{-1} . The amplitude on the vertical axis is normalized to a maximum frequency spectrum of 0 dB.

A large amplitude difference can be observed between the healthy motor and all the three fault conditions (H–HS5, H–HS10, and H–HS15). When the faults on the bearings were compared (HS5–HS10–HS15), the amplitude difference

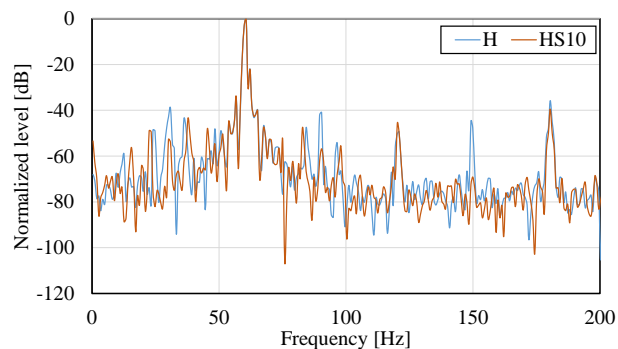


Fig. 5. Spectral analysis of H–HS10 at 1765 min^{-1} .

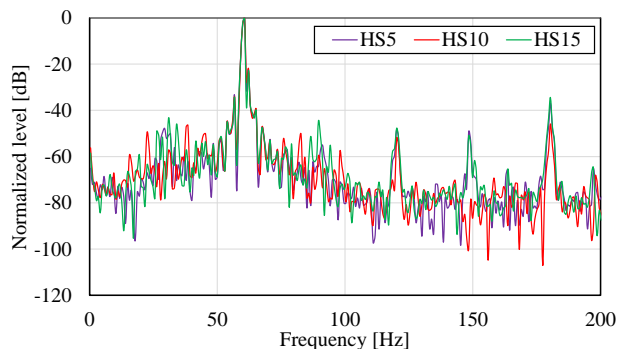


Fig. 6. Spectral analysis of HS5–HS10–HS15 at 1765 min^{-1} .

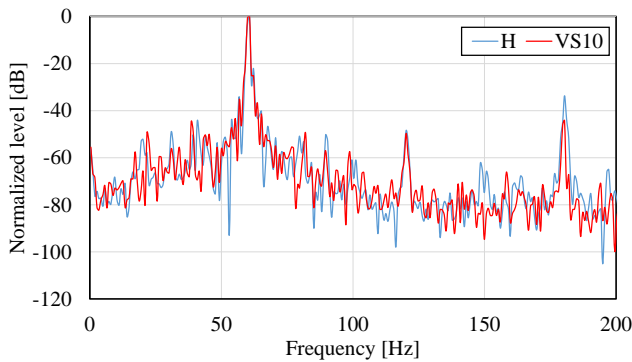
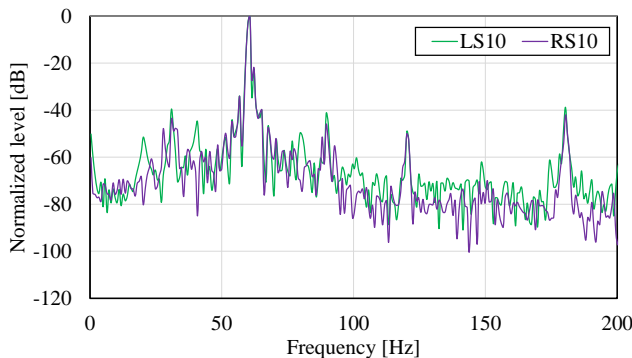
observed was sufficient to differentiate the cases. Amplitude differences in the frequency components were clearly visible at frequencies of 30, 90, 150, and 180 Hz. At 30 and 90 Hz, amplitude changes were observed at all rotating speeds (1780 , 1775 , 1770 , and 1765 min^{-1}). At 150 and 180 Hz, in contrast, no significant amplitude change was observed when the speed was varied, under any of the four bearing conditions. Frequencies of 30 and 90 Hz were therefore used in the study. This allowed differences between the healthy and faulty conditions and between different fault conditions to be localized.

When a pit is induced on a bearing, a shock wave with a characteristic frequency is generated. The frequency mainly depends on the point at which the fault is induced and the level of damage. The analysis performed in the present study assumed a scratch to be similar to a pit. Characteristic frequencies of 30 and 90 Hz were used to detect the bearing condition and were used to plot the feature distribution for more detailed study.

B. Spectral Analysis of Distinct Orientation of Bearing Failure

FFT analysis of the U-phase load current was performed for all bearing conditions (H, HS10, VS10, RS10, and LS10). Frequency spectra were plotted for H–VS10, LS10–RS10, and HS10–VS10 at a rotating speed of 1765 min^{-1} , and they are shown in Figs. 7 to 9.

If it is possible to differentiate the healthy motor from the four faulty motors, it should also be possible to localize the differences among the faulty motors. As with the progression


 Fig. 7. Spectral analysis of H-VS10 at 1765 min⁻¹.

 Fig. 8. Spectral analysis of LS10-RS10 at 1765 min⁻¹.

analysis, amplitude differences were observed at 30 and 90 Hz at all rotating speeds. This further confirmed the generation of a shock wave pulse, appearance of a characteristic frequency, and changes in the load current value of the stator, suggesting a relationship between scratching, load current, characteristic frequency, and shock wave pulse generation. To establish the precise relationship and derive the governing equations, a more detailed research will be needed.

C. Justification for the changes at the 30 and 90 Hz

Heretofore exploration was done to identify the reason for the magnitude changes at the 30 and 90 Hz. Coincidentally, similar amplitude changes had been observed in the case of eccentricity fault. The frequencies monitored for detecting the eccentricity fault were 25 and 75 Hz (approximately) with the power supply frequency of 50 Hz [30]. Indeed, the analytical calculation was performed considering the power supply frequency to be 60 Hz, correspondingly the eccentricity fault detection frequencies are not observed at 30 and 90 Hz.

Hence the frequency spectrum of bearing faults was no longer in relation with eccentricity fault and imperatively a brief study is required to find the reason why the amplitude changes are observed at the noticed frequency for all the rotating speed. There is a reason for the emergence of amplitude changes at the frequencies 30 and 90 Hz. In the case of a four-pole induction motor, the synchronous speed N_s is 1800 min⁻¹. Thus, the motor rotates at 30 revolutions per second with an associated frequency of 30 Hz. The 60 Hz frequency of the power supply is independent of the 30 and 90 Hz frequencies. Since the power supply is fed directly from the

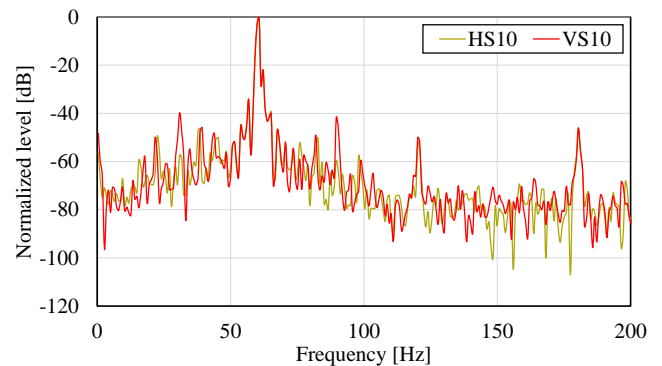
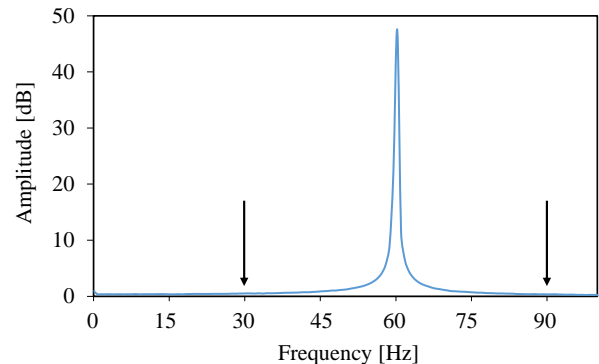

 Fig. 9. Spectral analysis of HS10-VS10 at 1765 min⁻¹.


Fig. 10. Spectral analysis of voltage (FFT).

main system, harmonic distortion is likely to appear in the voltage. For clarification, horizontal scratch 10 mm bearing condition was selected and the spectral analysis (FFT) of voltage was accomplished. Fig. 10 clearly discloses the fact that no signals are observed at the frequencies 30 and 90 Hz and thus they do not affect the bearing failure analysis. The other bearing failure conditions also show similar observation (H, HS5, HS15, VS10, LS10, and RS10). The rotating speed of the induction motor and the two signals (30 and 90 Hz) that appear in the frequency spectrum of the stator load current as sideband fundamental frequency components play important roles. In the present study, for example, the motor rotated at 1765/60 (revolutions/sec) had a value of 29.41 Hz. At this rotational speed, two signals will appear in the spectrum of the load current. The frequencies of these signals FB are given as follows:

$$F_B = F_L \pm F_R \quad (1)$$

where F_L is the frequency of the power supply (60 Hz) and F_R is the frequency calculated from the rotating speed. Thus, for example, rotating speeds of 1780, 1775, 1770, and 1765 min⁻¹ give values of 29.66, 29.58, 29.50, and 29.41 Hz, respectively. At 1765 min⁻¹, the frequencies FB are 30.59 Hz (60–29.41 Hz) and 89.41 Hz (60 + 29.41 Hz).

The frequency of the current spectrum is known to change with the rotating speed. However, in the present study, the changes in the amplitude of the load current always had frequencies of 30 and 90 Hz irrespective of the rotating speed. This was an artifact of the low frequency resolution (0.76 Hz)

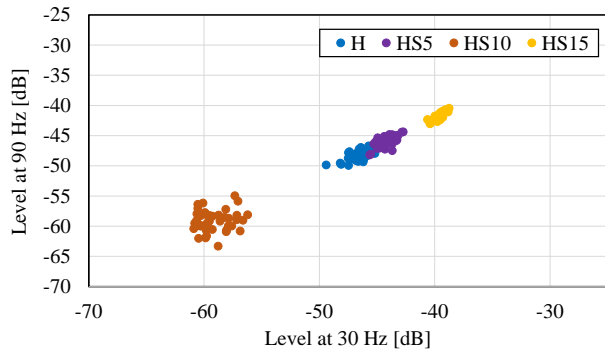


Fig. 11. Feature distribution of progressive bearing failure analysis at 1770 min^{-1} .

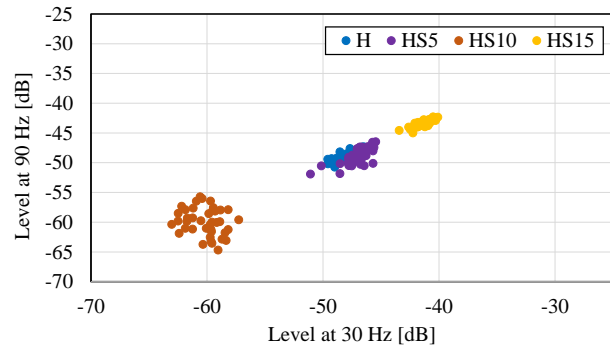


Fig. 12. Feature distribution of progressive bearing failure analysis at 1765 min^{-1} .

of the measuring equipment and made it impossible to discriminate between the changes observed at the frequencies of the current spectrum. The 30 and 90 Hz frequency components therefore play a significant role in the spectral analysis.

V. FEATURE DISTRIBUTION ANALYSIS

In feature distribution analysis, the amplitude of 30 and 90 Hz characteristic frequencies were plotted two-dimensionally for the analysis of both fault progression and orientation.

A. Progressive Bearing Failure

In both healthy and faulty motors, the contribution of each feature was evaluated from the load condition. In this section, we discuss four bearing conditions (H, HS5, HS10, and HS15). Under each condition, the location distinguishing behavior depends on the rotating speed of the motor and the bearing conditions. Figs. 11 and 12 show the feature distribution at rotating speeds of 1770 and 1765 min^{-1} for all bearing conditions, respectively. Even when overlaps occurred, the bearing conditions fell into distinctive classes, allowing them to be differentiated. When scratches of similar type with different dimensions were analyzed, their location corresponded to their class, suggesting that size plays an important role. Conditions HS10 and HS15 could be clearly distinguished from the healthy motor. In contrast, an overlap between HS5 and the healthy motor made it possible to derive only a partial evaluation of the condition. The proposed method could identify bearing failure while the motor was running. This allows a fault to be identified

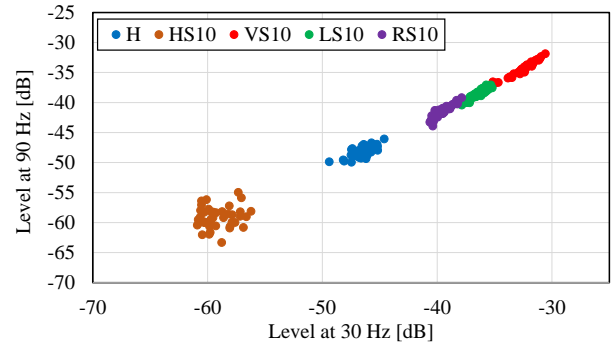


Fig. 13. Feature distribution of distinct orientation failure analysis at 1770 min^{-1} .

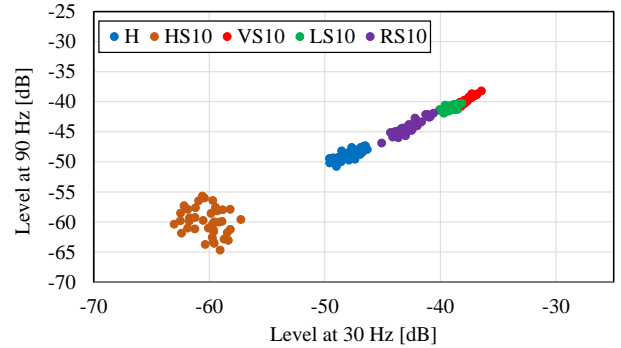


Fig. 14. Feature distribution of distinct orientation failure analysis at 1765 min^{-1} .

at any stage in the working life and demonstrates the significant role that feature distribution plays in the analysis of progressive bearing failure.

B. Classification of Distinct Orientation

In this section, we analyze the five bearing conditions (H, HS10, VS10, RS10, and LS10). These were again classified according to their class of location and distinguishing behavior. Figs. 13 and 14 show the feature distribution for all conditions at rotating speeds of 1770 and 1765 min^{-1} , respectively. With the exception of HS10, the scratches were located adjacently. Even when overlaps occurred, it was possible to differentiate between scratch types. Scratches of the same size but with different orientations showed a distinctive behavior. The orientation was shown to play a significant role, allowing the orientation to be identified. To fully understand the relationship between factors, a more detailed research will be necessary. However, the study confirmed that feature distribution plays an important role in identifying the orientation of bearing failures.

VI. PROPOSED METHOD FOR DIAGNOSING BEARING FAILURE

In this section, we introduce the use of SVM for detecting the progression and orientation of bearing failures. SVM is a pattern recognition method that has been used to classify objects into categories [31]. SVM belongs to the group of linear classification methods but can also perform non-linear classification. This is done using a kernel function, mapping high input operators with high dimensional features. SVM

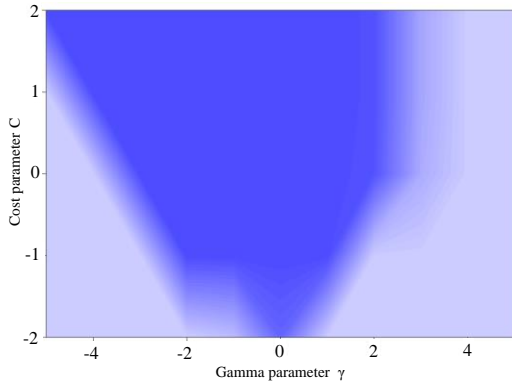


Fig. 15. Accuracy rate function between cost parameter and gamma parameter.

TABLE I
SUPPORT VECTOR MACHINE DESCRIPTION

Type of SVM	Soft Margin SVM
Kernel	Radial Basis Function Kernel
Cost parameter, C	1.0
Gamma parameter, γ	0.333
Number of support vectors	8
Number of classes	2

uses soft margins and hard margins. The SVM type and its usage are determined by the linearity condition. This study applied non-linear classification so that the soft margin matched the prescribed condition. In Soft Margin SVM, cost parameter C is introduced, which controls the trade-off between maximizing the margin and minimizing the training error. If the value of C is lower, it tends to emphasize the margin, ignoring the outliers in the training data. Contrarily, larger C value tends to overfit the training data. Besides, Radial Basis Function kernel is also used commonly as gamma parameter γ and the boundary decision is established. Smaller γ value leads to a simple decision boundary and vice-versa. Thus, both the cost parameter and gamma parameter play a significant role and their tuning are accomplished.

In the present work, initially data were divided into eight groups, the first seven of which provided training data. Data from group eight were used for evaluation. By alternating the groups, seven group diagnosis accuracy rates were obtained, and the average was calculated. The process was repeated for the different values of C and γ . Fig. 15 shows the two-dimensional map plotted against the accuracy rate function involving cost parameter C and gamma parameter γ . The higher accuracy rate was obtained in the deep blue color portion by varying the values of C and γ . TABLE I summarizes the SVM specification handled for present study of bearing failure diagnosis. Programming was done using R language software.

A. Diagnosis Scheme

The SVM-based diagnosis was carried out for two various factors, namely, fault progression and orientation, using the amplitude of the 30 and 90 Hz characteristic frequency components. The accuracy rate was derived as follows:

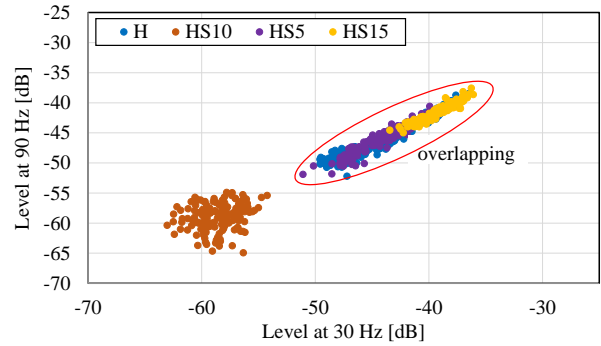


Fig. 16. Integrated progressive analysis.

$$\text{Accuracy rate (\%)} = \frac{\text{Number of data diagnosed properly}}{\text{Total number of data used for diagnosis}} \times 100 \quad (2)$$

To mimic an industrial environment, the diagnosis was conducted without considering the rotating speed of the induction motor.

B. Diagnosis of Progressive Bearing Failure

The analysis considered four types of bearing condition. For conditions H–HS5, H–HS10, and H–HS15, 320 sets of load current data were used. Each dataset had both 30 and 90 Hz amplitude frequency components. From the 320 sets, 240 were used as training data, and the remaining 80 were used as evaluation data. For H–HS5–HS10–HS15, 640 sets of loads current data were used, with 480 used as training data and the remaining 160 used as evaluation data. Four rotating speeds (1780, 1775, 1770, and 1765 min⁻¹) were considered.

TABLE II shows the accuracy rate when diagnosing progressive bearing failure. The accuracy rates for H–HS10 and H–HS15 were sufficiently high to be considered acceptable in practical applications. In the case of H–HS5, the accuracy rate was lower because of a significant overlapping between the healthy and faulty conditions (Figs. 11 and 12). The tests confirmed that the method can predict bearing failure in a running motor. However, it is unsuitable to the detection of minor failures.

In the analysis of H–HS5–HS10–HS15, Fig. 16 plots the four bearing conditions feature without considering the rotation speed. Significant overlaps were found between the different bearing conditions, making the diagnosis process tedious. However, the bearing condition was identified with an average accuracy rate of 83.13% and the proposed method was effective in localizing the difference between four conditions, demonstrating its ability to produce a diagnosis, even when overlapping was encountered. This is a significant advantage of the proposed method, making it suitable for use at different speeds and in industrial environments. overlapping was encountered. This is a significant advantage of the proposed method, making it suitable for use at different speeds and in industrial environments.

C. Diagnosis of Orientation

The diagnosis of orientation similarly took no account of rotational speed. For conditions H–HS10, H–VS10, H–LS10,

TABLE II
SCRATCH PROGRESSION DIAGNOSIS RESULT

Bearing Condition	Accuracy Rate (%)
H-HS5	73.75
H-HS10	100
H-HS15	92.5
H-HS5-HS10-HS15	83.13
Average	87.35

TABLE III
DISTINCT ORIENTATION DIAGNOSIS RESULT

Bearing Condition	Accuracy Rate (%)
H-HS10	100
H-VS10	96.25
H-LS10	90
H-RS10	87.5
H-HS10-VS10-LS10-RS10	74.75
Average	89.7

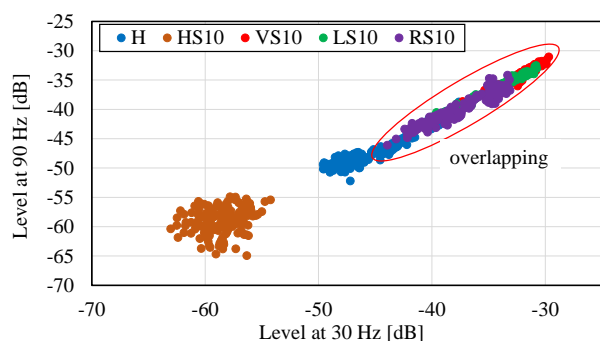


Fig. 17. Unified distinct orientation analysis.

and H-RS10, 320 sets of load current data were used, each with amplitude frequency components of 30 and 90 Hz. Of these, 240 were used as training data, and the remaining 80 were used as evaluation data. In the case of H-HS10-VS10-LS10-RS10, 800 sets of load current data were obtained, with 600 used as training data and the remaining 200 used for evaluation. Four rotating speeds (1780, 1775, 1770, and 1765 min^{-1}) were considered.

Fig. 17 plots the five bearing conditions feature, without considering the rotation speed. TABLE III shows the accuracy rate of H-HS10, H-VS10, H-LS10, H-RS10, and H-HS10-VS10-LS10-RS10. The average accuracy rate of 89.7% was considered acceptable for practical applications. The diagnosis rate was again high even when overlapping was encountered. Outer raceway scratches in all orientations were diagnosed satisfactorily, demonstrating the ability of this approach to investigate the orientation of a bearing failure. This suggests that the method can be applied in real industrial settings.

D. Diagnosis Taking Account of the Rotating Speed

An additional diagnosis was also performed for both fault progression and orientation, considering the rotating speed of the induction motor. An average accuracy rate of 95% was achieved across the four rotating speeds, demonstrating that the

proposed method can yield satisfactory results when considering the rotation speed of the motor.

VII. CONCLUSION

The progression and orientation of outer raceway bearing scratches were investigated using FFT analysis. Further diagnosis was performed using an SVM. To mimic the use of motors in industrial environments, the diagnosis was performed without considering the rotating speed of the motor. The performance of the proposed system was verified in laboratory experiments.

A horizontal scratch 5 mm in length was partially diagnosed, and a full diagnosis was achieved with scratches 10 mm in length. This demonstrated that the proposed method was able to monitor the progression of bearing failures of 10 mm or more. Test on the orientation of the fault demonstrated that scratches in all orientations could be detected. The proposed method was therefore shown to be suitable for industrial applications. Detection, diagnosis, and analysis could be carried out without taking into account the rotating speed of the induction motor.

The proposed method was shown to have the following advantages:

- * The problem of overlapping is largely eliminated.
- * The proposed system can be applied at different speeds.
- * When the rotating speed of the induction motor was taken into account, a high level of diagnostic accuracy was obtained.

In a future work, we will apply this method to the damaged bearing available in the industry. We also intend to test the method for converter fed electrical machines and on the other types of industrial motor.

ACKNOWLEDGMENT

The authors would gratefully acknowledge the contributions of Mr. Makoto Masuko, Mr. Toshiaki Matsumura and Mr. Keisuke Akahori during the experimental work and data analysis.

REFERENCES

- [1] O. V. Thorsen and M. Dalva, "A survey of faults on induction motors in offshore oil industry, petrochemical industry, gas terminals, and oil refineries," *IEEE Transactions on Industrial Applications*, vol. 31, no. 5, pp. 1186-1196, 1995.
- [2] Y. J. Kim, S. H. Hong, T. S. Kong and H. D. Kim, "On-Site Application of Novel Partial Discharge Monitoring Scheme for Rotating Machine," *Electrical Insulation Conference (EIC)*, pp. 85-88, Washington, USA, June 2015.
- [3] X. Jin, M.H. Azarian, C. Lau, L.L. Cheng, and M. Pecht, "Physics-of failure analysis of cooling fan," *PHM-Shenzhen Conference*, pp. 1-8, China, May 2011.
- [4] W. Wang and M. Pecht, "Economic analysis of canary-based prognostics and health management," *IEEE Transactions on Industrial Electronics*, vol. 58, no. 7, pp. 3077-3089, Jul. 2011.
- [5] M. Cococcioni, B. Lazzerini, and S.L. Volpi, "Robust diagnosis of rolling element bearings based on classification techniques," *IEEE Transactions on Industrial Informatics*, vol. 9, no. 4, pp. 2256-2263, Nov. 2013.
- [6] M.D.Prieto, G.Cirincione, A.G. Espinosa, J. Ortega, and H. Henao, "Bearing fault detection by a novel condition-monitoring scheme based on statistical-time features and neural networks," *IEEE Transactions on Industrial Electronics*, vol. 60, no. 8, pp. 3398-3407, Aug. 2013.
- [7] R.B. Randall, "Vibration-based condition monitoring: Industrial, Aerospace and Automotive Application," Wiley, Chichester, U.K, pp. 24-65, pp. 167-227, Jan. 2011.

- [8] G. C. Stone, "Condition Monitoring and Diagnostics of Motor and Stator windings – A Review," IEEE Transaction on Dielectric and Electric Insulation, vol. 20, no. 6, pp. 2073-2080, Dec. 2013.
- [9] J. Cusido, L. Romeral, J. A. Ortega, J. A. Rosero, and A. Garvia Espinosa, "Fault Detection in Induction Machines Using Power Spectral Density in Wavelet Decomposition," IEEE Transaction on Industrial Electronics, vol. 55, no. 2, pp. 633-643, Jan. 2008.
- [10] O. A. Mohammed, N. Y. Abed, and S. Ganu, "Modeling and Characterization of Induction Motor Internal Faults Using Finite Element and Discrete Wavelet Transforms," IEEE Transaction on Magnetics, vol. 42, no. 10, pp. 3434-3436, Sep. 2006.
- [11] Valeria C. M. N. Leite, J. G. B. da Silva, G. F. Cintra Veloso, L. E. B. da Silva, "Detection of Localized Bearing Faults in Induction Machines by Spectral Kurtosis and Envelope Analysis of Stator Current," IEEE Transactions on Industrial Electronics, vol. 62, no. 3, pp. 1855-1865, Mar. 2015.
- [12] Christelle Piantsof Mbo'o, Kay Hameyer, "Fault diagnosis of bearing damage by means of the linear discriminant analysis of stator current features from the frequency selection," IEEE Transactions on Industrial Applications, vol. 52, no. 5, pp. 3861-3868, 2016.
- [13] Jason R. Stack, Thomas G. Habetler, and Ronald G. Harley, "Fault Signature Modeling and Detection of Inner-Race Bearing Faults," IEEE Transactions on Industrial Applications, vol. 42, no.1, pp. 61-67, Jan/Feb. 2006.
- [14] W. Zhou, B. Lu, T. Habetler, and R. Harley, "Incipient bearing fault detection via motor stator current noise cancellation using wiener filter," IEEE Transactions on Industry Applications, vol. 45, no. 4, pp. 1309-1317, July/Aug. 2009.
- [15] M. Delgado, G. Cirrincione, A. Garcia, J. Ortega, and H. Henao, "A novel condition monitoring scheme for bearing faults based on curvilinear component analysis and hierarchical neural networks," ICEM2012 - XXth International Conference on Electrical Machines, pp. 2472-2478, Sept. 2012.
- [16] X. Jin, M. Zhao, T. Chow, and M. Pecht, "Motor bearing fault diagnosis using trace ratio linear discriminant analysis," IEEE Transactions on Industrial Electronics, vol. 61, no. 5, pp. 2441-2451, May 2014.
- [17] S. A. S. A. Kazzaz and G. Singh, "Experimental investigations on induction machine condition monitoring and fault diagnosis using digital signal processing techniques," Electric Power Systems Research, vol. 65, pp. 197-221, 2003.
- [18] R. H. C. Pala'cios, A. Goedel, W. F. Godoy, and J. A. Fabri, "Fault identification in the stator winding of induction motors using pca with artificial neural networks," Journal of Control, Automation and Electrical Systems, vol. 27, no. 4, pp. 406-418, Aug. 2016.
- [19] M. Seera, C. P. Lim, D. Ishak, and H. Singh, "Offline and online fault detection and diagnosis of induction motors using a hybrid soft computing model," Applied Soft Computing, vol. 13, no. 12, pp. 4493-4507, 2013.
- [20] J. Rosero, L. Romeral, E. Rosero, and J. Urresty, "Fault detection in dynamic conditions by means of discrete wavelet decomposition for pmsm running under bearing damage," in APEC 2009 - Twenty-Fourth Annual IEEE Applied Power Electronics Conference and Exposition, pp. 951-956, Feb. 2009.
- [21] F. Immovilli, M. Cocconcelli, A. Bellini, and R. Rubini, "Detection of generalized-roughness bearing fault by spectral-kurtosis energy of vibration or current signals," IEEE Transactions on Industrial Electronics, vol. 56, no. 11, pp. 4710-4717, Jun. 2009.
- [22] J. Antoni, "Fast computation of the kurtogram for the detection of transient faults," Mechanical System Signal Processing, vol. 21, no. 1, pp. 108-124, Jan. 2007.
- [23] Valeria C.M.N. Leite, Jonas Guedes Borges da Silva, Giscard Francimeire Cintra Veloso, "Detection of Localized Bearing Faults in Induction Machines by Spectral Kurtosis and Envelope Analysis of Stator Current," IEEE Transactions on Industrial Electronics, vol. 62, no. 3, pp. 1855-1865, Mar. 2015.
- [24] N. Sawalhi, "Rolling element bearings: Diagnostic, prognostic and fault simulations," Ph.D. dissertation, Faculty Engineering of Mechanical and Manufacturing Engineering, University of New South Wales, Sydney, Australia, 2007.
- [25] D. Siegel, C. Ly, and J. Lee, "Methodology and framework for predicting helicopter rolling element bearing failure," IEEE Transaction on Reliability, vol. 61, no. 4, pp. 846-857, Dec. 2012.
- [26] T. W. Chow and H.-Z. Tan, "HOS-based nonparametric and parametric methodologies for machine fault detection," IEEE Transactions on Industrial Electronics, vol. 47, no. 5, pp. 1051-1059, Oct. 2000.
- [27] L. Zhen, H. Zhengjia, Z. Yanyang, and C. Xuefeng, "Bearing condition monitoring based on shock pulse method and improved redundant lifting scheme," Mathematics and Computers in Simulation, vol. 79, no. 3, pp. 318-338, Dec. 2008.
- [28] J. K. Sinha and K. Elbhah, "A future possibility of vibration based condition monitoring of rotating machines," Mechanical System and Signal Processing, vol. 34, no. 1, pp. 231-240, Jan. 2013.
- [29] Shrinathan Esakimuthu Pandarakone, Keisuke Akahori, Toshiki Matsumura, Yukio Mizuno, and Hisahide Nakamura, "Development of a Methodology for Bearing Fault Scrutiny and Diagnosis using SVM," in ICIT 2017 18th Annual IEEE International Conference on Industrial Technology, Toronto, Canada, pp. 282-287, Mar. 2017.
- [30] M. Blodt, J. Regnier and J. Faucher, "Distinguishing Load Torque Oscillations and Eccentricity Faults in Induction Motors Using Stator Current Wigner Distributions," IEEE Transactions on Industrial Applications, vol. 45, no. 6, pp. 1991-2000, Nov/Dec. 2009.
- [31] K. B. Liplowits and T. R. Cundari, "Applications of Support Vector Machines in Chemistry", Reviews in Computational Chemistry, vol. 23, chap. 6, 2007.



Shrinathan Esakimuthu Pandarakone (S'16) was born in Nagercail, India, on September 20, 1992. He received the Bachelor of Engineering degree (B.E) in Electrical and Electronics Engineering from Anna University, India in 2014. During his bachelor course, he was honored for his achievements and performances. Also, he received the Master of Science (M.Sc.) degree in the Department of Engineering Physics, Electronics and Mechanics from Nagoya Institute of Technology, Japan in 2017. Currently, he is pursuing his Doctor of Philosophy (Ph.D.) at Nagoya Institute of Technology in the Department of Electrical and Mechanical Engineering.

He is performing his research in fault diagnosis of electrical machines, condition monitoring and failure detection of low voltage facilities.

Mr. Esakimuthu Pandarakone is a student member of the Institute of Electrical Engineers of Japan (IEEJ).

Yukio Mizuno (M'90) was born in Nagoya, Japan, in 1958. He received the B.Sc., M.Sc., and Ph.D. degrees, all in electrical engineering from the Nagoya University, Nagoya, Japan in 1981, 1983, and 1986, respectively.

From 1986 to 1993, he was employed as a Research Assistant at the Toyohashi University of Technology, Toyohashi, Japan. In 1993, he joined Nagoya Institute of Technology, Nagoya, Japan as an Associate Professor at the Department of Electrical and Computer Engineering and was promoted to a Professor in 2003. He is now a Professor of Graduate School of Engineering, Nagare College, Nagoya Institute of Technology. He has been engaged in the research on electrical insulation diagnosis, high voltage insulation, superconducting power cable, quantification of power frequency electric, and magnetic fields, etc.

Prof. Mizuno is a member of the Institute of Electrical Engineers of Japan, Cryogenic Association of Japan and CIGRE.

Hisahide Nakamura (M'02) was born in Yamaguchi, Japan, in 1971. He received the B.E and M.E degrees in Electrical and Computer Engineering from Nagoya Institute of Technology in 1995 and 1997, respectively, and the Ph.D. degree in Electrical Engineering from Nagoya University in 2002.

From 1997 to 1999, he worked for FANUC LTD. In 2002, he joined TOENEC Corporation. His research interests are fault diagnosis of electrical machines.

Dr. Nakamura is a member of the Institute of Electrical Engineers of Japan, the Institute of Electrical Installation Engineers of Japan, the Institute of Systems, Control and Information Engineers, Information Processing Society of Japan, and the Society of Instrument and Control Engineers.

